

# Control Algorithm for ISTsat-1

Diogo Pessanha Neves  
d.pessanha.neves@tecnico.ulisboa.pt

Instituto Superior Técnico, Universidade de Lisboa, Portugal

July 2019

## Abstract

The ISTsat-1 is a cubesat satellite developed by students from Instituto Superior Técnico (IST) under the ESA educational program Fly Your Satellite. The objective of this mission is to monitor and characterize the ADS-B signals from aircraft. One of the priorities of the satellite platform is to point it into the desired direction with a certain level of accuracy to accomplish the mission as well as to ensure the satellite does not get excessive rotation. This work focus the development of the Attitude Determination and Control System which will ensure these conditions. The system was developed to be integrated into the physical platform previously designed for the onboard computer. The challenge to surpass is to ensure the satellite reaches the pointing requirements posed by the payload while using a low-cost and low-power platform. To evaluate the possible solutions the tool Simulink was used, allowing to model the satellite and the environment to which the satellite will be subject. Afterwards, the problem was studied using computational light attitude estimation algorithms. Then, the attitude determination solutions allowed to study control solutions also focused on computational efficiency. The results show it is possible to use quick, efficient and low-cost solutions to develop satellites with low orientation requirements.

**Keywords:** Satellite, CubeSat, ISTsat, Attitude, Estimation, Control, Magnetic Actuation

## 1. Introduction

The ISTsat-1 satellite is the first satellite mission of a group of students from the Instituto Superior Técnico called NanoSat. The purpose of this mission is to study the Automatic Dependent Surveillance-Broadcast (ADS-B) signals from low earth orbit (LEO).

ISTsat-1 payload antenna was designed to cover a 600 km diameter area and it needs the satellite pointing to NADIR in order to be able to characterize the ADS-B signals thus, it was established the error in pointing should be less than 20°. At 400 km this error limit corresponds to a deviation of 145.6 km from the NADIR point. Lastly, there are some concerns regarding the tumbling after being launched and while not pointing to NADIR. Consequently, the ADCS must have a mode where it only reduces the excess of angular rotation. So detumbling should be able to stop spinning rates at least up to 30°/s. For the satellite to be able to point to NADIR it must have a reference of its own attitude relative to the Earth therefore the ADCS must also estimate the attitude. The permissible error in the attitude estimation must ensure the satellite pointing accuracy is still within the established limit.

## 2. Modelling

### 2.1. Dynamics

For referencing we operate with four coordinate frames: ECI, ECEF, ORBIT and BODY. Per definition [10] the attitude will represent the satellite own coordinate frame BODY in the inertial Earth frame ECI. The rotation from ECI to BODY is represented by a quaternion.

$$\mathbf{q} = [\eta \ \epsilon_1 \ \epsilon_2 \ \epsilon_3]^T \quad (1)$$

The change in the satellite attitude quaternion can be represented as a function of the satellite angular rate  $\boldsymbol{\omega}$  relative to the Earth inertial frame.

$$\dot{\mathbf{q}} = \frac{1}{2} \Omega(\boldsymbol{\omega}) \mathbf{q} \quad (2)$$

$$\Omega(\boldsymbol{\omega}) = \begin{bmatrix} 0 & -\boldsymbol{\omega}^T \\ \boldsymbol{\omega} & \boldsymbol{\omega} \times \end{bmatrix} \quad (3)$$

To complete the connection between the attitude and resulting torque we relate the angular rate change through time to the actuating torques of the satellite.

$$\dot{\boldsymbol{\omega}} = J^{-1} (\boldsymbol{\tau}_t - \boldsymbol{\omega} \times J \boldsymbol{\omega}) \quad (4)$$

Where  $\boldsymbol{\tau}_t$  is the sum of all the torques actuating the satellite. To have a more precise model this

sum includes aerodynamic effects, residual magnetic dipoles and gravity gradient effects besides the control generated to control the satellite attitude. To compute these effects three models needed to be included into the simulator: EGM2008 for detailed gravity representation, CIRA72 for atmosphere density and IGRF12 for the Earth magnetic characterization. These three models compute their respective environment quantities with regard to the satellite position in the ECEF frame.

## 2.2. Sensors & Actuators

Each one of three sensors the ADCS uses, gyro, magnetometer and coarse sun sensor, were modelled and included into the simulator to included the measuring errors. The corrupted observations are represented by the accentuated variables:  $\hat{\boldsymbol{\omega}}$ ,  $\hat{\mathbf{B}}$  and  $\hat{\mathbf{S}}$ .

The gyroscope used by the ADCS is embedded in the low cost IMU chip: MPU9250. Its model was based on [4], which besides the misalignment error  $G_g$ , random angular rate error  $\mathbf{n}_{arw}$  and bias error  $\boldsymbol{\beta}_g$  also includes the gyro bias drift rate  $\mathbf{n}_{rrw}$ .

$$\hat{\boldsymbol{\omega}} = [G_g]\boldsymbol{\omega} + \boldsymbol{\beta}_g + \mathbf{n}_{arw} \quad (5)$$

$$\dot{\boldsymbol{\beta}}_g = \mathbf{n}_{rrw} \quad (6)$$

The magnetometer sensor used is a low cost chip fabricated by Honeywell, HMC5983 which provides 3 axis readings. Its model is a simplified version of the gyro, which does not include the bias drift.

$$\hat{\mathbf{B}} = [G_B]\mathbf{B} + \boldsymbol{\beta}_B + \mathbf{n}_B \quad (7)$$

The coarse sun sensor is formed by five photodiodes assembled into each solar panel. The photodiodes actually work like a phototransistor, the more sunlight it receives the more current it allows to flow from anode to cathode. The CSS model was based on [13] which estimates the sun direction based on the current flowing in each diode relative to the reference current  $i_0$ .

$$\hat{\mathbf{S}}_B = \frac{1}{i_0} \begin{bmatrix} i_{+x} - i_{-x} \\ i_{+y} - i_{-y} \\ i_{+z} - i_{-z} \end{bmatrix} \quad (8)$$

$$i = i_0 \cos \alpha + n_{ss} \quad (9)$$

The random error of the current reading is represented by  $n_{ss}$ . The angle  $\alpha$  is the angle the sunlight makes with the normal face of the photodiode solar panel. This angle is set to 90 if the photodiode has no line of sight to the sun like in eclipse or if it is facing the opposite direction.

To control the attitude, the ADCS uses magnetorquers. These devices are controlled coils that interact with the Earth magnetic field when induced with a electric current resulting in a torque. The

torque generated through this effect  $\boldsymbol{\tau}_c$  can be modelled as:

$$\boldsymbol{\tau}_c = \mathbf{m}_c \times \mathbf{B}_B \quad (10)$$

Where  $m_c$  is the magnetic dipole the coils are capable of producing. Using three of these devices, each align with different axis is possible to generate any magnetic dipole. However, using these devices do not allow to produce torque in the magnetic flux vector direction.

## 3. Attitude Determination Algorithms

The approach to the attitude estimation problem started by using static methods discarding any dynamic model knowledge. The most used algorithms TRIAD, QUEST, SVD and FOAM were selected, knowing the last three are direct results from Wahba's formulation of the attitude problem.

### 3.1. TRIAD

TRIAD uses two measurements  $\mathbf{b}_1$  and  $\mathbf{b}_2$  to build a orthonormal triaxial space and uses the inverse transformation of the reference measurements  $\mathbf{r}_1$  and  $\mathbf{r}_2$  to compute the attitude matrix.

$$A = [\mathbf{w}_1 \ \mathbf{w}_2 \ \mathbf{w}_3] \cdot [\mathbf{v}_1 \ \mathbf{v}_2 \ \mathbf{v}_3]^T \quad (11)$$

$$\mathbf{w}_1 = \mathbf{b}_1 \quad (12)$$

$$\mathbf{w}_2 = \mathbf{b}_1 \times \mathbf{b}_2 \quad (13)$$

$$\mathbf{w}_3 = \mathbf{w}_1 \times \mathbf{w}_2 \quad (14)$$

$$\mathbf{v}_1 = \mathbf{r}_1 \quad (15)$$

$$\mathbf{v}_2 = \mathbf{r}_1 \times \mathbf{r}_2 \quad (16)$$

$$\mathbf{v}_3 = \mathbf{v}_1 \times \mathbf{v}_2 \quad (17)$$

### 3.2. QUEST

The formulation for the other three solutions started from the same equation and it presents the problem as a weighted cost function  $L$  that each solution tries to minimise.

$$L(A) = \lambda_0 - \text{tr}(AB^T) \quad (18)$$

$$B = \sum_{k=1}^n a_k \mathbf{r}_k \cdot \mathbf{b}_k^T \quad (19)$$

$$\lambda_0 = \sum_{k=1}^n a_k \quad (20)$$

Where  $k$  is the number of measurements and  $a_k$  is the weight of the  $k^{\text{th}}$  observation. With this, Davenport [7] proved the cost function could be turned into a eigenvalue/eigenvector equation by creating a matrix  $K$ .

$$K\hat{q} = \lambda_{max}\hat{q} \quad (21)$$

The matrix is generated using the  $B$  matrix and the external product between observation measure-

ments and their respective references.

$$K = \begin{bmatrix} B + B^T - \text{tr}(B) \cdot I & z \\ z^T & \text{tr}(B) \end{bmatrix} \quad (22)$$

$$z = \sum_{k=1}^n a_k (b_k \times r_k) \quad (23)$$

The second algorithm tested is QUEST from [11], which iteratively estimates the solution for the eigenvector problem using a polynomial equation  $\psi$ .

$$\psi(\lambda) = \det(\lambda I_{4 \times 4} - K) \quad (24)$$

### 3.3. SVD

Instead of an iterative model, in [8] a cleaner solution is achieved using the singular value matrix decomposition (SVD) of the  $B$  matrix to generate two orthonormal matrices  $U$  and  $V$ .

$$B = U S V^T \quad (25)$$

Then using those matrices it computes the attitude matrix.

$$\hat{A} = U \cdot \text{diag}([1 \ 1 \ M]) \cdot V \quad (26)$$

$$M = \det(U) \cdot \det(V) \quad (27)$$

### 3.4. FOAM

Another matrix focused solution is the Fast Optimal Attitude Matrix (FOAM) [9], which avoids the decompositions proposed in SVD. The attitude estimation equation results into a simplified version of the SVD:

$$\begin{aligned} \hat{A} &= \left( \frac{a_1}{\lambda_{max}} \right) (b_1 r_1^T + (b_1 \times b_\times)(r_1 \times r_\times)^T) \\ &+ \left( \frac{a_2}{\lambda_{max}} \right) (b_2 r_2^T + (b_2 \times b_\times)(r_2 \times r_\times)^T) \\ &+ b_\times r_\times \end{aligned} \quad (28)$$

Where  $\lambda_{max}$  will be given by:

$$\lambda_{max} = \sqrt{\|B\|_F^2 + \|r_1 \times r_2\| \|b_1 \times b_2\|} \quad (29)$$

$$\|B\|_F^2 = a_1^2 + a_2^2 + 2a_1 a_2 (r_1 \cdot r_2)(b_1 \cdot b_2) \quad (30)$$

### 3.5. Enhanced QUEST

After understanding these static solutions, the dynamic algorithms were focused in seeking to bring more accuracy and stability to the solutions. Among the available dynamic solutions three of the lightest solutions were studied: Enhanced QUEST, Extended Kalman Filter and the Explicit Complementary Filter.

The EQUEST method presented in [2] uses the solution from QUEST  $\mathbf{q}_q$  and the solution from a

quaternion propagator  $\tilde{\mathbf{q}}$  in a dynamic weight filter to achieve a filtered quaternion estimation  $\hat{\mathbf{q}}$ .

$$\hat{\mathbf{q}} = (1 - \beta) \cdot \tilde{\mathbf{q}} + \beta \cdot \mathbf{q}_q \quad (31)$$

Where the dynamic weight  $\beta$  is computed according to the collinearity between measurements and eclipse state upon which  $\beta_0 = 0$ .

$$\beta = (1 - |\mathbf{r}_1 \cdot \mathbf{r}_2|^2) \beta_0 \quad (32)$$

### 3.6. MEKF

The Multiplicative Extended Kalman Filter is an evolution of the Kalman Filter [?][12][3][10]. Based on the linearisation of the satellite model at the instant  $k$  it updates the attitude error with a rotation quaternion built upon the measurements. A special feature of the Kalman filter is the use of a state covariance matrix to compute the residual error.

$$H_k = \begin{bmatrix} (A(\hat{q}_k^-) r_1)_\times & 0_{3 \times 3} \\ (A(\hat{q}_k^-) r_2)_\times & 0_{3 \times 3} \end{bmatrix} \quad (33)$$

$$K_k = P_k^- H_k [H_k P_k^- H_k^T + R]^{-1} \quad (34)$$

With this gain, the previous state is updated using the residual measurement error  $z_k$ .

$$z_k = \begin{bmatrix} \tilde{b}_1 \\ \tilde{b}_2 \end{bmatrix}_{3 \times 1} - \begin{bmatrix} A(\hat{q}_k^-) \cdot [r_1]_{3 \times 1} \\ A(\hat{q}_k^-) \cdot [r_2]_{3 \times 1} \end{bmatrix} \quad (35)$$

$$\hat{x}_k^+ = \hat{x}_k^- + K_k z_k \quad (36)$$

$$(37)$$

Then the attitude quaternion and gyro bias are updated with the resulting state  $\hat{x}_k^+$ .

$$\hat{q}_k^* = \delta q_k (\delta \hat{v}_k^+) \otimes \hat{q}_k^- \quad (38)$$

$$\beta_g|_k = \beta_g|_{k-1} + \delta \beta_g|_k \quad (39)$$

Finally, the covariance matrix  $P$  is also updated.

$$P_k^+ = [I - K_k H_k] P_k^- [I - K_k H_k]^T \quad (40)$$

### 3.7. Explicit Complementary Filter

The Explicit Complementary Filter [6][5] fuses the gyroscope data with the observations to follow the evolution of the attitude quaternion through time.

$$\gamma = \sum k_i (\mathbf{b}_i \times A(\hat{\mathbf{q}}) \mathbf{r}_i) \quad (41)$$

$$\dot{\hat{\mathbf{q}}} = \Omega(\hat{\omega}_B - \beta_g + k_p \gamma) \otimes \hat{\mathbf{q}} \quad (42)$$

$$\dot{\hat{\beta}}_g = -k_g \gamma \quad (43)$$

Where  $\gamma$  is the correction coefficient,  $k_p$  a quaternion gain,  $k_g$  a gyroscope bias gain and  $k_i$  is the observation relative gain.

#### 4. Attitude Control Algorithms

The ADCS will work with two modes, one for rotational energy dissipation and other for pointing to NADIR. The first state will be called detumbling and is initiated every time the satellite has an angular rate above  $5^\circ/s$  and the second called pointing shall be where the satellite will be most of the time. Due to the constrain of being in a plane orthogonal to the magnetic flux direction, the torque generated by the magnetorquers cannot always be equal to the desired torque. The projection of the desired torque results from the magnetic dipole  $m_b$  orthonormal to the desired torque and magnetic flux plane.

$$m_b = \frac{\mathbf{B} \times \boldsymbol{\tau}_d}{|\mathbf{B}|^2} \quad (44)$$

##### 4.1. Detumbling

For the detumbling three algorithm options were studied, two based on the magnetic flux derivative and another based upon the gyroscope measurements. The first method called B-dot [1], feeds the magnetic flux derivative to compute the necessary magnetic dipole  $m_b$ .

$$m_b = -k_b \dot{\mathbf{B}} \quad (45)$$

A variation of this method, also presented in the bibliography, could be written based on a bang bang controller where the output magnitude is fixed to  $m_{max}$  and the signal is established by the magnetic flux derivative.

$$m_b = -m_{max} \cdot \text{sign}(\dot{\mathbf{B}}) \quad (46)$$

The gyro-feedback is similar to B-dot but using the gyroscope readings instead of the magnetometer.

$$m_b = -k_b \boldsymbol{\omega} \quad (47)$$

These solutions are not global asymptotic stable because the Lyapunov functions candidates are zero whenever the angular rate vector is aligned with the magnetic flux vector. However, in [1] this situation was proven to be a non issue as the controller does not converge during these periods but does not diverge either and they are transitory situations.

##### 4.2. Pointing

The pointing controller will use the orbit frame to operate as the third coordinate axis is aligned with NADIR direction. Thus a new attitude quaternion  $\mathbf{q}_o$  will be generated to represent the BODY coordinate frame orientation in the ORBIT frame using the rotation to ORBIT from ECI represented by  $\mathbf{q}([R_{\mathcal{O}}^{\mathcal{E}}])$ .

$$\mathbf{q}_o = \mathbf{q}([R_{\mathcal{O}}^{\mathcal{B}}]) = \mathbf{q} \otimes \mathbf{q}([R_{\mathcal{O}}^{\mathcal{E}}]) \quad (48)$$

The control is based on proportional derivative controller where the error feedback will be computed through the quaternion error. However instead of using the derivative of the quaternion error is preferable to use the already available gyro readings. Using  $k_\epsilon$  and  $k_\omega$  as the proportional and derivative gains respectively the desired torque  $\boldsymbol{\tau}_d$  can be written as:

$$\boldsymbol{\tau}_d = -(k_\epsilon \delta \mathbf{q}_\epsilon + k_\omega \boldsymbol{\omega}) \quad (49)$$

The vector  $\mathbf{q}_\epsilon$  represents the imaginary part of the error quaternion  $\delta \mathbf{q}$ . The attitude reference written in the ORBIT frame is equal to the identity quaternion and therefore the quaternion error is equal to the inverse of the satellite attitude written in ORBIT.

$$\delta \mathbf{q} = \mathbf{q}_d \otimes \mathbf{q}_o^{-1} \quad (50)$$

$$\mathbf{q}_d = [1000]^T \quad (51)$$

The stability of the PD controller is proven in [10] using the following Lyapunov function  $V$ :

$$V = \frac{1}{4} \boldsymbol{\omega}_{\mathcal{B}}^T J \boldsymbol{\omega}_{\mathcal{B}} + \frac{1}{2} k_p \left( \delta \mathbf{q}_\epsilon \delta \mathbf{q}_\epsilon^T + (1 - \delta \mathbf{q}_\eta)^2 \right) \quad (52)$$

#### 5. Results

From the initial simulations we established the estimated heading error for each sensor in different situations. Using the specifications from the data-sheet provided by the manufacturer, the magnetometer sensor presents a heading error around  $0.56^\circ$ . The sun sensor performance depends upon how many photodiodes are lighted. Assuming a  $120^\circ$  field of vision there is a blind zone induced by the absence of a solar panel in the  $-Z$  face.

Photodiodes	0	1	2	3
RMSE ( $^\circ$ )	-	34.7	19.2	$7.1 \times 10^{-4}$
Coverage (%)	3.0	39.7	52.1	5.2

Table 1: Sun sensor RMSE and spherical coverage by the number of lighted photodiodes

##### 5.1. Attitude Estimation

Method	RMSE ( $^\circ$ )	$E_{max}$ ( $^\circ$ )
TRIAD	34.97	179.997
SVD	22.57	179.992
QUEST	23.33	179.936
FOAM	31.92	179.919

Table 2: Deterministic algorithms error results when the satellite is lightened

The maximum error of the algorithms results from the near collinearity between the two observations. In these cases where the angular proximity was below  $15^\circ$  the results were too unstable. Another problem found was the error induced by the CSS low accuracy which still posed a problem even after trying to mitigate the influence with sensor weighted compensation. When the sensor had less than two photodiodes lighted the error rose significantly.

The dynamic solutions proposed tried to solve both these problems, the attitude estimation instability and not being able to estimate the attitude during eclipse.

Adding the simple EQUEST filter to the QUEST method produced very good results during the daylight phase of the orbit. However during the eclipse the estimation error drifted around. EQUEST pre-

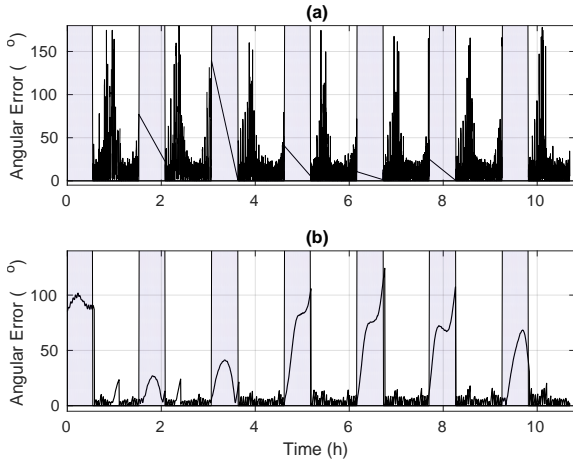


Figure 1: Comparison between the angular error of QUEST (a) and EQUEST (b) during 7 orbits simulation (shaded regions indicate eclipse instances).

sented a  $RMSE$  near  $35^\circ$  and a maximum error was reduced to  $125^\circ$ . However during the daylight time of the orbit the error was maintain below  $25^\circ$ .

The MEKF does not present the same problems during the propagation of the attitude during the eclipse phase of the orbit. The continuous use of the magnetometer to update the attitude and the bias estimation allowed to obtain more accurate results during the eclipse. Due to the CSS heterogeneous behaviour three covariance matrices were created for the three scenarios where at least one photo diode is lighted. With the MEKF it was possible to achieve a  $RMSE$  around  $8^\circ$  and a great reduction of the maximum error to  $42.9^\circ$  after a stabilization period. The estimation of the gyroscope bias error with the MEKF was kept under  $15\ mdeg/s$ .

The less complex ECF also went some gain customization in order to lessen the disruptive effect of the CSS. Compared to the MEKF the ECF was also

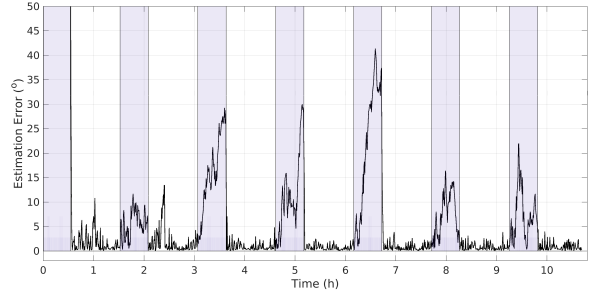


Figure 2: Angular error of the MEKF for 7 orbital revolutions simulation (shaded regions indicate eclipse instances).

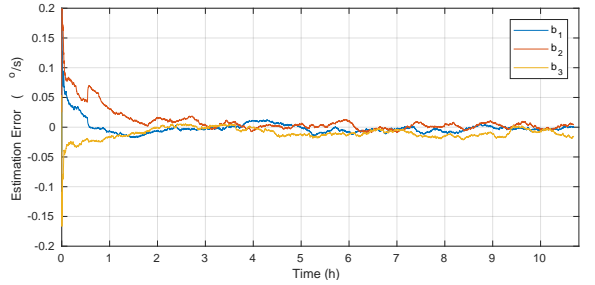


Figure 3: MEKF gyro bias estimation error in the 3 body axis ( $b_1$ ,  $b_2$ ,  $b_3$ ) for 7 orbital revolutions simulation (shaded regions indicate eclipse instances).

able to achieve good stability in the attitude estimation bringing the  $RMSE$  down to less than  $7^\circ$  and presented a maximum error of  $25^\circ$ . Even though the

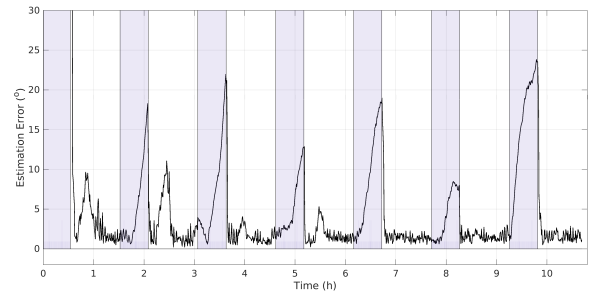


Figure 4: Angular error of the ECF for 7 orbital revolutions simulation (shaded regions indicate eclipse instances).

gyroscope bias estimation error was not as good as the MEKF they were kept under  $61\ mdeg/s$  during the simulations with an average value around  $22\ mdeg/s$ .

## 5.2. Detumbling

The simulation of detumbling was made by setting four study cases with different orbits, where the first also started with an angular rate of  $15^\circ/s$  while the other three used an angular rate of  $30^\circ/s$ .

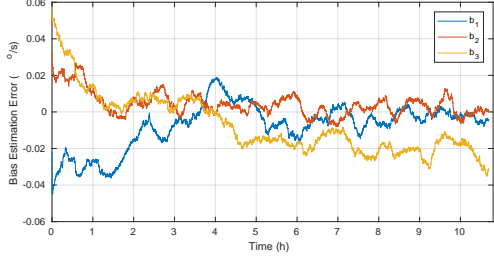


Figure 5: ECF gyro bias estimation error in the 3 body axis ( $b_1$ ,  $b_2$ ,  $b_3$ ) for seven orbital revolutions simulation (shaded regions indicate eclipse instances).

Case	Parameter	B-dot	Bang-Bang	Gyro
1	$\Delta t$ (s)	217	1006	230
1	$\Delta E$ (J)	50	38	47
2	$\Delta t$ (s)	17182	2094	7170
2	$\Delta E$ (J)	774	82	485
3	$\Delta t$ (s)	390	4030	392
3	$\Delta E$ (J)	161	150	133
4	$\Delta t$ (s)	332	2255	313
4	$\Delta E$ (J)	132	84	105

Table 3: Detumbling controllers simulation results

For most of the simulated cases the gyro-feedback performance was similar to the b-dot while revealing an improved energy consumption by saving up to 18% relative to the b-dot. The lower output limit of the bang-bang is evident in most simulation cases where it presented a slower pace to reach the threshold than the other two. However it generally uses less energy than the other solutions and the power demand is much lower than the other two options. The time anomalies present in case 2 using the b-dot and gyro-feedback solutions are pinned on the alignment of the magnetic flux vector with the angular rate. The same occurred during the simulation of the third case using the bang-bang solution.

### 5.3. Pointing

The pointing controller simulations were made using the output results from the ECF algorithm. The simulations initial conditions were defined assuming the satellite will begin the pointing mode after passing through the detumbling mode. This would validate the initial angular rate equal to the detumbling algorithm lower angular rate limit of  $0.8^\circ/s$ . Lastly the control sampling time was setted to  $0.5$  s. The use of the ECF attitude output introduces an error into the control references during the initial instances of the simulation. After receiving the first sunlight rays, we can see in 5.3 the pointing error diminish and maintained it below the  $20^\circ$  during

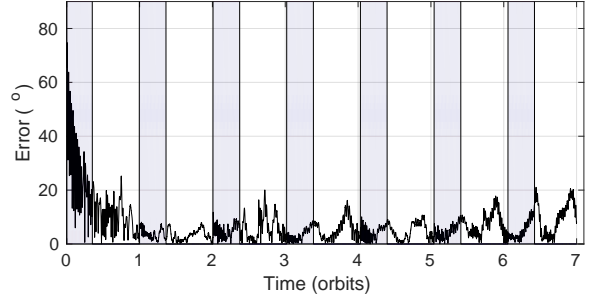


Figure 6: Pointing controller simulation angular error throughout 7 orbits (shaded regions indicate eclipse instances).

7 orbits (10h30). So in average, the simulations demonstrated the controller takes around half orbit to get the z axis within  $20^\circ$  of the NADIR alignment and after the first orbit it stays above this performance level for 99.7% of the simulated time. The more difficult level below  $10^\circ$  pointing error was achieved during 87.45% after the satellite first orbit revolution and the for at least half the time the pointing error was kept under the  $5^\circ$  limit. During

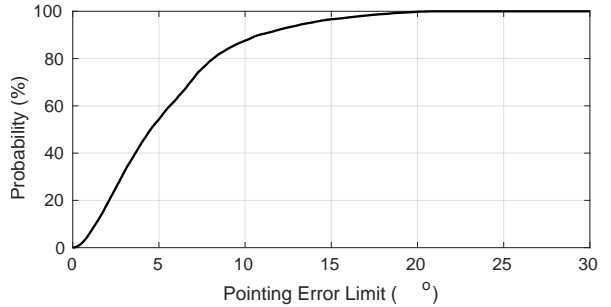


Figure 7: Cumulative probability function of the pointing controller error.

these control simulations the PD shown an average power consumption around  $6$  mW after stabilization which is below the budget allocation of  $39$  mW. The peak consumption of  $233$  mW was reached during the first orbit.

## 6. Conclusions

From the results of this work, the CSS configuration used demonstrated that is only good enough when more than two photodiodes are lighted. Due to this, the static attitude estimators QUEST, TRIAD, FOAM and SVD are not adequate for this satellite for they cannot ensure a stable enough attitude estimation necessary to perform the necessary attitude control. Among the dynamic algorithms the best choice is the ECF because it offers the better attitude estimation performance than the EQUEST and similar to the MEKLF while being simpler than

the MEKF.

From the detumbling results the bang-bang option had a slower but more efficient response. The rate it spends energy allows the EPS to replenish its battery and maintain it charged for most of the time. Concerning safety and robustness during the detumbling the bang-bang variation of the  $\dot{b}$  would be the most adequate controller.

Lastly, for 99.7% of the simulated time the pointing controller, even using the attitude estimation provided by the ECF, achieved a total pointing accuracy below  $20^\circ$ . The slow control suits the ISTsat-1 discrete actuation as the low proportional gain also results in less overshooting near the NADIR reference axis and offers a more tight control over the angular rate avoiding excessive rotation problems.

### Acknowledgements

The author would like to thank the professors Paulo Oliveira and Rui Rocha for their support and guidance. Also would like to thank to the ISTsat-1 team for their friendship and commitment to the project.

### References

- [1] G. Avanzini and F. Giuliotti. Magnetic detumbling of a rigid spacecraft. *Journal of Guidance, Control, and Dynamics*, 35:1326–1334, 07 2012.
- [2] J. L. Crassidis, S. F. Andrews, F. L. Markley, and K. Ha. Contingency designs for attitude determination of TRMM. Technical report, NASA, 1995.
- [3] J. L. Crassidis, F. L. Markley, and Y. Cheng. Survey of Nonlinear Attitude Estimation Methods. *Journal of Guidance, Control, and Dynamics*, 30(1):12–28, 2007.
- [4] Q. Lam, N. Stamatakos, C. Woodruff, and S. Ashton. Gyro Modeling and Estimation of Its Random Noise Sources. *AIAA Guidance, Navigation, and Control Conference and Exhibit*, (June), 2003.
- [5] R. Mahony, T. Hamel, P. Morin, and E. Malis. Nonlinear complementary filters on the special linear group. *International Journal of Control*, 85(10):1557–1573, 2008.
- [6] R. Mahony, T. Hamel, and J. M. Pflimlin. Complementary filter design on the special orthogonal group  $SO(3)$ . *Proceedings of the 44th IEEE Conference on Decision and Control, and the European Control Conference, CDC-ECC '05*, 2005(1):1477–1484, 2005.
- [7] F. Markley and D. Mortari. Quaternion attitude estimation using vector observations. *Journal of the Astronautical Sciences*, 48(2):359–380, 2000.
- [8] F. L. Markley. Attitude Determination using Vector Observations and the Singular Value Decomposition. *The Journal of the Astronautical Sciences*, 36(3):245–258, 1988.
- [9] F. L. Markley. Attitude determination using vector observations - A fast optimal matrix algorithm. *The Journal of the Astronautical Sciences*, 41(2):261–280, 1993.
- [10] F. L. Markley and J. L. Crassidis. *Fundamentals of Spacecraft Attitude Determination and Control*. Springer-Verlag New York Inc., 2014.
- [11] M. D. Shuster and S. D. Oh. Three-axis attitude determination from vector observations. *Journal of Guidance, Control, and Dynamics*, 1981.
- [12] D. Simon. *Optimal State Estimation: Kalman,  $H_\infty$ , and Nonlinear Approaches*. 2006.
- [13] Y. Winetraub, S. Bitan, U. Dd, and A. Heller. Attitude Determination – Advanced Sun Sensors for Pico-satellites. *Tel-Aviv University*, pages 1–10.